

# e-MERLIN and VLBI observations of the luminous infrared galaxy IC 883: a nuclear starburst and an AGN candidate revealed

C. Romero-Cañizales<sup>1,2,\*</sup>, M. A. Pérez-Torres<sup>1</sup>, A. Alberdi<sup>1</sup>, M. K. Argo<sup>3,4</sup>, R. J. Beswick<sup>4</sup>, E. Kankare<sup>2</sup>, F. Batejat<sup>5</sup>, A. Efstathiou<sup>6</sup>, S. Mattila<sup>2</sup>, J. E. Conway<sup>5</sup>, S. T. Garrington<sup>4</sup>, T. W. B. Muxlow<sup>4</sup>, S. D. Ryder<sup>7</sup>, and P. Väisänen<sup>8</sup>

<sup>1</sup> Instituto de Astrofísica de Andalucía - CSIC, PO Box 3004, 18008 Granada, Spain

<sup>2</sup> Tuorla Observatory, Department of Physics and Astronomy, University of Turku, Väisälantie 20, FI-21500 Piikkiö, Finland

<sup>3</sup> Netherlands Institute for Radio Astronomy (ASTRON), Postbus 2, 7990 AA Dwingeloo, The Netherlands

<sup>4</sup> Jodrell Bank Centre for Astrophysics, Alan Turing Building, School of Physics and Astronomy, The University of Manchester, Manchester M13 9PL

<sup>5</sup> Onsala Space Observatory, SE-439 92 Onsala, Sweden

<sup>6</sup> School of Sciences, European University Cyprus, Diogenes Street, Engomi, 1516 Nicosia, Cyprus

<sup>7</sup> Australian Astronomical Observatory, PO Box 296, Epping, NSW 1710, Australia

<sup>8</sup> South African Astronomical Observatory, PO Box 9, Observatory 7935, South Africa

Received June 17, 2021; accepted ?

## ABSTRACT

**Context.** The high star formation rates of luminous infrared galaxies (LIRGs) make them ideal places for core-collapse supernova (CCSN) searches. Massive star formation can often be found in coexistence with an active galactic nucleus (AGN), contributing jointly to the energy source of LIRGs. At radio frequencies, free from dust extinction, it is possible to detect compact components within the innermost LIRG nuclear regions, such as SNe and SN remnants, as well as AGN buried deep in the LIRG nuclei.

**Aims.** Our study of the LIRG IC 883 aims at: (i) investigating the parsec-scale radio structure of the (circum-)nuclear regions of IC 883; (ii) detecting at radio frequencies the two recently reported circumnuclear SNe 2010cu and 2011hi, which were discovered by near-IR (NIR) adaptive optics observations of IC 883; and (iii) further investigating the nature of SN 2011hi at NIR wavelengths.

**Methods.** We used the e-EVN at 5 GHz, and e-MERLIN at 6.9 GHz, to observe contemporaneously the LIRG IC 883 at high angular-resolution (from tens to hundreds of milliarcsec) and with high sensitivity ( $< 70 \mu\text{Jy}$ ), complemented by archival VLBI data at 5 and 8.4 GHz. We also used the Gemini-North telescope to obtain late-time *JHK* photometry for SN 2011hi.

**Results.** The circumnuclear regions traced by e-MERLIN at 6.9 GHz have an extension of  $\sim 1$  kpc, at a position angle of  $130^\circ$ , and show a striking double-sided structure, which very likely corresponds to a warped rotating ring, in agreement with previous studies. Our e-EVN observations at 5 GHz and complementary archival VLBI data at 5 GHz and 8.4 GHz, reveal the presence of various milliarcsec compact components in the nucleus of IC 883. A single compact source, an AGN candidate, dominates the emission at both nuclear and circumnuclear scales, as imaged with the e-EVN and e-MERLIN, respectively. The other milliarcsec components are very suggestive of ongoing nuclear CCSN activity. Our e-EVN observations also resulted in upper limits to the radio luminosity of the two SNe in IC 883 recently discovered at NIR wavelengths. We refine the classification of SN 2011hi as a Type IIP SN according to our latest Gemini-North epoch from 2012, in agreement with a low-luminosity radio SN nature. We estimate a CCSN rate lower limit of  $1.1_{-0.6}^{+1.3} \text{ yr}^{-1}$  for the entire galaxy, based on three nuclear radio SNe and the circumnuclear SNe 2010cu and 2011hi.

**Key words.** Galaxies: starburst – Galaxies: nuclei – Galaxies: individual: IC 883 – Radio continuum: stars – Radiation mechanisms: non-thermal – supernovae: individual: SN 2010cu, SN 2011hi

## 1. Introduction

The excess of radio continuum and infrared (IR) emission in luminous IR galaxies (LIRGs) is associated with vigorous formation of massive stars ( $M \gtrsim 8 M_\odot$ ) and/or an active galactic nucleus (AGN) (see e.g., Sanders & Mirabel 1996). Core-collapse supernovae (CCSNe) serve as probes of the star formation rate (SFR) of massive stars, and therefore their detection in LIRGs is a pertinent task.

IC 883 is a LIRG with IR luminosity ( $L_{\text{IR}} = L[8-1000 \mu\text{m}] \sim 4.7 \times 10^{11} L_\odot$ ) at a distance of 100 Mpc (1 mas  $\approx 0.48$  pc), according to Sanders et al. (2003). This LIRG is probably the result of the merger of two disk galaxies (Smith et al. 1995), as suggested by its associated tidal tails: a diffuse one approximately perpendicular to the region where gas and dust prefer-

entially concentrate (i.e., the disk) as seen in optical and near-IR (NIR) studies (e.g., Smith et al. 1995; Scoville et al. 2000; Modica et al. 2012), and a narrow one along the disk itself (Keel 1985).

Taking  $L_{\text{IR}}$  as a measure of the rate at which massive stars are formed, results in a corresponding CCSN rate,  $\nu_{\text{SN}}$ , of  $\sim 1.3 \text{ yr}^{-1}$  for IC 883 (assuming the empirical relation obtained by Mattila & Meikle 2001). Optical spectroscopic studies by Veilleux et al. (1995) have led to the classification of the IC 883 nucleus as a low-ionisation narrow emission-line region. However, Yuan et al. (2010) have recently reclassified this galaxy as a composite starburst-AGN, based on the revised optical diagnostic diagrams by Kewley et al. (2006). The multi-wavelength study on IC 883 by Modica et al. (2012) also supports a composite nature. Consequently it is expected that an AGN is contributing to the total  $L_{\text{IR}}$  in IC 883, and thus the  $\nu_{\text{SN}}$  should be lower than  $1.3 \text{ yr}^{-1}$ . Indeed, at radio frequencies,

\* e-mail: crroca@utu.fi

Smith et al. (1998) and Parra et al. (2010) have found evidence of compact AGN activity through VLBI studies of IC 883.

IC 883 is part of our program “An ALTAIR study of Supernovae in Luminous Infrared Galaxies”, using Gemini-North with its Laser Guide Star adaptive optics (AO) system (e.g., Kankare et al. 2008). During the four year survey, our program has yielded the discovery of two CCSNe in IC 883 within a 12-month period: SN 2010cu (24 Feb. 2010, Ryder et al. 2010) and SN 2011hi (11 Feb. 2011, Kankare et al. 2011). Kankare et al. (2012) concluded that either a Type IIP or a II<sub>n</sub>/L SN provided the best fits to the NIR light curves of SNe 2010cu and 2011hi.

In this paper we report our radio observations towards the nuclear and circumnuclear regions of IC 883, as well as the most recent NIR epoch obtained with Gemini-North on January 31 2012, not included in Kankare et al. (2012). In Section 2 we give details of our radio and NIR observations, Section 3 contains our results and discussion, and Section 4 contains the summary of our study.

## 2. Observations

IC 883 was observed at radio frequencies with the electronic Multi-Element Remotely Linked Interferometer Network (e-MERLIN) and with the electronic European very long baseline interferometry (VLBI) Network (e-EVN<sup>1</sup>), and at NIR wavelengths with the Gemini-North telescope. Our observations aimed at imaging the parsec-scale radio structure of the (circum-)nuclear regions of IC 883, and detecting SNe 2010cu and 2011hi at radio frequencies, as well as to further investigating the nature of SN 2011hi at NIR wavelengths. To complement our radio observations, we have also analysed publicly available archival VLBI data.

In Table 1 we give some details on the observational parameters of the different radio observations included in our study: e-MERLIN, e-EVN and additional VLBA and EVN observations.

### 2.1. e-MERLIN observations and data reduction

We carried out e-MERLIN observations of IC 883 at 6.9 GHz (median central frequency) on 19 March 2011. These were Director’s Discretionary Time (DDT) observations within the commissioning phase of e-MERLIN, which included the following 25 m diameter antennas: Mark II, Defford, Knockin, Darnhall and Pickmere. The observations lasted ~ 24 hr, from which approximately 20 were spent on target and 10 hr were ultimately usable after editing. Four sub-bands (512 channels each) with dual polarisation were used, accounting for a total bandwidth of 512 MHz.

We analysed the data within the NRAO Astronomical Image Processing System (AIPS). 3C286 set the absolute flux density scale following an iterative process. The flux estimated for 3C286 in the shortest baseline (Mark II-Pickmere), at the centre of the different sub-bands, was on average 5.56 Jy. We then calibrated the amplitude of DA 193, which is a bright and unresolved source as seen by all e-MERLIN baselines, resulting in an average flux density of 3.72 Jy. Finally, we used DA 193 to set the flux density of the phase reference source, J1324+3622, which resulted in an average flux density of 68.25 mJy. We performed

<sup>1</sup> The development of e-VLBI within the EVN has been made possible via EXPReS project funded by the EC FP6 IST Integrated Infrastructure Initiative contract # 026642 - with a goal to achieve 1 Gbps e-VLBI real-time data transfer and correlation.

a series of phase-only self-calibration iterations of the phase reference source, before phase-calibrating the target source. To account for the correlation offset from the position of the strongest source in the field, we used the task UVSUB in AIPS. To improve the sensitivity, we performed phase-only self-calibration iterations on the target source. We achieved a thermal rms noise in the IC 883 map of 44  $\mu$ Jy/beam, for a beam size of 165×88 mas at  $-11.6^\circ$  (see left panel in Figure 1), obtained with natural weighting and ROBUST=1 within AIPS.

### 2.2. e-EVN observations and data reduction

We observed IC 883 on 23 March 2011 (ToO project: RR006, P.I.: Romero-Cañizales) at 5 GHz, with the e-EVN, which included the following antennas (diameter, location): Effelsberg (100 m, Germany), Mark II (25 m, UK), Medicina (32 m, Italy), Onsala (25 m, Sweden), Torun (32 m, Poland), Westerbork array (14×25 m, NL) and Yebes (40 m, Spain).

RR006 was a 2 hr experiment (~1.3 hr, total time on source), recorded at 1024 Mbps using eight sub-bands, each of 16 MHz and dual polarisation. The data were correlated at the EVN MkIV Data Processor at JIVE with an averaging time of 2 s. The point-like source J1159+2914 (2.45 Jy at 5 GHz) was used as a fringe finder and bandpass calibrator. J1317+3425 (0.35 Jy at 5 GHz), at  $\sim 0.7^\circ$  angular distance from IC 883, served as phase reference source. 3.4 min scans on IC 883 were alternated with 1.2 min scans on J1317+3425. The data were analysed with AIPS. We also used the Caltech program DIFMAP (Shepherd et al. 1995) to image the calibrators and to assess the performance of each antenna.

In an attempt to detect a radio counterpart for SN 2011hi, its coordinates derived from the NIR images were used for pointing and correlation. A local rms of  $\sim 30 \mu$ Jy/beam was achieved at the pointing centre. Since no radio source was detected above  $3\sigma$  at that position, we corrected the visibility data with the task UVSUB in AIPS, as we did for the e-MERLIN data, to account for the correlation offset from the position of the strongest source in the field, i.e., to the radio nucleus of IC 883. The shift of  $\sim 0.8$  arcsec is well within the primary beam of each antenna in the used array.

For the imaging process within AIPS we used different weighting schemes in order to test the reliability of our results. Due to the scarce uv-coverage, the use of natural weighting tends to give rise to secondary side lobes at a 60 per cent level of the main lobe, which can produce artifacts in the reconstruction imaging process that can be confused with putative sources. Our final image was made using uniform weighting and ROBUST=1. We achieved a final thermal rms in the map of 66.2  $\mu$ Jy/beam, for a beam size of 9.20×6.36 mas at  $-76.1^\circ$  (see Figure 1, right panel).

### 2.3. Archival VLBI data

We have analysed Very Long Baseline Array (VLBA) data from projects BN026 and BN027 at 5 GHz, and BC196 at 8.4 GHz. The VLBA observations under program BC196 were processed with the DiFX VLBI correlator (Deller et al. 2011). We also report EVN observations at 5 GHz made on June 15th 2006 (project: EP055, P.I.: R. Parra); see Table 1.

In project EP055, IC 883 was observed in four scans spread over 24 hr to optimize the uv-coverage for a total observation time on source of  $\sim 1.3$  hr. The array used comprised 10 EVN stations: Lovell (76 m, UK), Cambridge (32 m, UK), Westerbork

**Table 1.** Observational parameters of the radio observations.

Epoch label	Project	Array	Observing date	$\nu$ (GHz)	Phase calibrator	$P_\nu$ (Jy/beam)	Weighting	Convolving beam (mas)	rms ( $\mu$ Jy/beam)
(1)	(2)	(3)	(4)	(5)	(6)	(7)	(8)	(9)	(10)
EM	-	e-MERLIN	2011-03-19	6.9	J1324+3622	0.07	N,1	165.23×88.35 at 11.6°	44.0
V1	BN026	VLBA	2004-08-13	5.0	J1317+3425	0.25	N,0	3.71×1.47 at -0.1°	84.7
V2	BN027	VLBA	2004-09-20	5.0	J1310+3220	1.41	N,1	3.48×1.65 at 17.6°	119.0
V3	BN027	VLBA	2005-07-11	5.0	J1310+3220	1.19	N,2	3.43×1.78 at 11.5°	107.0
V4	EP055	EVN	2006-06-15	5.0	J2333+3901	0.81	U,1	7.99×6.00 at -81.3°	162.0
V5	RR006	e-EVN	2011-03-23	5.0	J1317+3425	0.35	U,1	9.20×6.36 at -76.1°	66.2
V6	BC196	VLBA	2011-05-15	8.4	J2330+3348	0.33	N,0	2.41×1.17 at -8.3°	174.0

**Notes.** Phase reference sources used in each observation are listed along with their associated peak intensities (columns 6 and 7). For the different IC 883 maps, column 8 lists the weighting parameters used in the imaging process: N=natural, U=uniform, and the number corresponds to the value of the ROBUST parameter). Column 9 lists the resolution, and column 10 the attained rms noise.

array (14×25 m, NL), Effelsberg (100 m, Germany), Medicina (32 m, Italy), Noto (32 m, Italy), Onsala (25 m, Sweden), Torun (32 m, Poland), Urumqi (25 m, China) and Shanghai (25 m, China). The observations were performed in a 1024 Mbps dual polarization mode. The data were correlated at JIVE in the Netherlands with an averaging time of 2 s.

All the additional VLBI data were edited and reduced using standard procedures within AIPS. The phase reference calibrator used in project BN027 is slightly resolved at VLBA scales, and we have thus corrected the fringe solutions from its structure. We did not apply any self-calibration to obtain the final images of IC 883. In the case of project EP055, the data from the two Chinese antennas (Ur and Sh) as well as from Cm could not be properly calibrated, so we omitted these antennas in the imaging process.

As in the case of our e-EVN epoch, we have tested the reliability of the sources in the different VLBI maps, by using different weighting schemes. We used the AIPS task UVSUB to apply shifts in  $\alpha$  and  $\delta$  to the visibility data on all the additional archival VLBI epochs. This allowed us to have all the maps centred at the same position ( $\alpha$ (J2000) = 13<sup>h</sup>20<sup>m</sup>35<sup>s</sup>.3184,  $\delta$ (J2000) = 34°08′22″352). Since the resulting images have a different convolving beam and were thus mapped with different pixel sizes, we changed their geometry to match that of our e-EVN epoch (pixel size of 0.5 mas), by means of the task OHGEO within AIPS.

#### 2.4. Gemini-North observations

Our Gemini-North observations of IC 883 were conducted with the ALTAIR Laser Guide Star AO system on the Near-Infrared Imager (NIRI). The LIRG was observed in 11 separate epochs between 2008 April 15.5 UT and 2012 January 31.6 UT, covering a period of 3.8 yr. Here we report the results from the most recent epoch of *JHK* imaging obtained in 2012 under program GN-2012A-Q-56 (P.I.: S. Ryder); the previous epochs are reported in Kankare et al. (2012). For details on the data reduction, calibration, image subtraction process and photometry of the ALTAIR/NIRI data on SN 2010cu and SN 2011hi we refer to Kankare et al. (2012).

Image subtraction based on the ISIS 2.2 (Alard & Lupton 1998; Alard 2000) package was used to compare the 2012 *JHK* images of IC 883 to the reference data obtained on 2010 May 4-5 UT. This revealed SN 2011hi to have faded below the detection limit of the Gemini images. Similar to deriving the *J*-band upper limit for SN 2010cu in Kankare et al. (2012) we used the QUBA package (see Valenti et al. 2011) running standard IRAF

tasks, to measure the faintest detectable sources in the 2010 reference image with poorer quality AO correction compared to the latest 2012 epoch. Taking into account the noise increasing by a factor of  $\sqrt{2}$  due to the image subtraction process, conservative  $5\sigma$  upper limits of roughly  $m_J > 19.7$  mag,  $m_H > 19.9$  mag, and  $m_K > 19.9$  mag were derived.

### 3. Results and discussion

The images of the nuclear and circumnuclear regions of IC 883 as observed with the e-EVN and e-MERLIN are shown in Figure 1. In Figure 2 we show the images resulting from a total of six VLBI epochs, covering a period of seven years. In Table 2 we report the estimated parameters for the  $> 5\sigma$  sources detected in all the images.

Our new Gemini-North epoch has yielded new *JHK* magnitude limits for SN 2011hi. In Figure 3 we show the SN 2011hi template light curve fits from Kankare et al. (2012), including the new limits obtained from our 2012 observations for comparison.

We note that the discovery of two SNe (2010cu and 2011hi) in a 3.8 yr period results in a  $\nu_{\text{SN}} \approx 0.5_{-0.3}^{+0.7} \text{ yr}^{-1}$  (using the upper and lower Poisson  $1\sigma$  uncertainties for two events given by Gehrels 1986), which agrees within the uncertainties with the IR luminosity-based CCSN rate of the galaxy. However, this estimate does not include any correction factors nor control time considerations, and should thus be regarded as a lower limit.

#### 3.1. The nature of SNe 2010cu and 2011hi

In Kankare et al. (2012) we investigated the nature of SNe 2010cu and 2011hi by means of five epochs of NIR photometric observations prior to 2012. Based on the comparison of the light curves of SN 2010cu and SN 2011hi to the CCSN templates presented in Mattila & Meikle (2001) and the well sampled NIR light curves of the canonical Type IIP SN 1999em (Krisciunas et al. 2009), it was concluded that the best fit for both SNe was either a Type IIP or a II<sub>n</sub>/L SN (see Kankare et al. 2012). The ordinary, linearly declining template fit was previously excluded because such fit suggested an extremely early discovery and an unrealistically long rise time to the light curve peak. A NIR-bright Type II<sub>n</sub>/L SN with  $\sim 0$  mag of extinction was favoured in Kankare et al. (2012) as the type of SN 2011hi due to the low ( $< 2$  mag) total line-of-sight extinction implied by the *J-K* colour map of the galaxy. However, a Type IIP light curve with higher extinction could also provide a good fit to the data, and as noted in Kankare et al. (2012), higher localized ex-

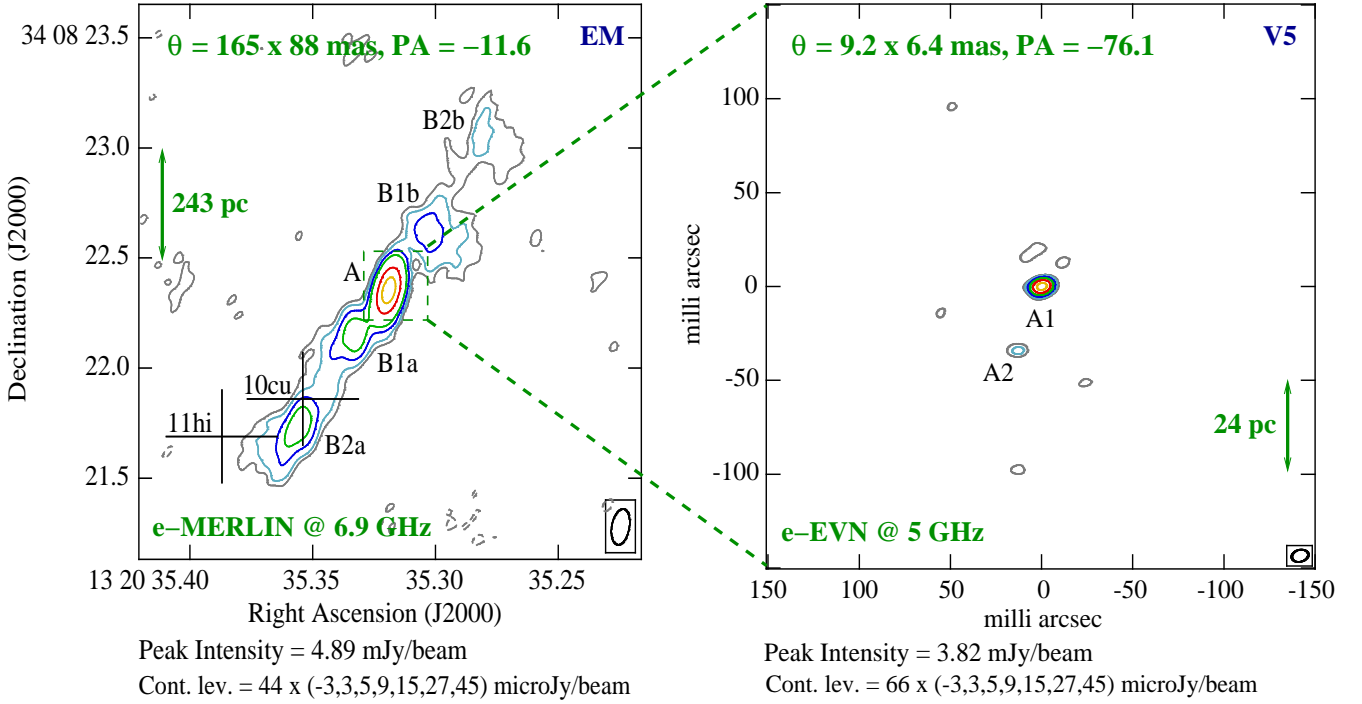


**Fig. 1.** IC 883 contour images at a median central frequency of 6.9 GHz obtained with e-MERLIN (left), and at 5 GHz with the e-EVN (right), in observations carried out in March 2011. The rms noise in the two images is 44 and 66  $\mu\text{Jy}/\text{beam}$ , respectively, and the convolving beam in each case is indicated the upper left corner of the maps. Dashed contours represent  $-3\sigma$  levels. Note that the brightest component at e-MERLIN scales is dominated by a compact source seen at mas scales with the e-EVN. The crosses in the left panel indicate the coordinates and positional errors of SNe 2010cu and 2011hi, according to the values reported in Kankare et al. (2012).

tinctions are possible, as the colour map is tracing only the large scale structures of the LIRG.

In Figure 3 we present the template  $\chi^2$  fits of the SN 2011hi light curves adopting the Calzetti et al. (2000) reddening law and including the new upper limits. However, these limits are not included in the fit, i.e., the values reported in the Table 2 of Kankare et al. (2012) are unchanged. Based on the new data, the slowly declining (NIR-bright Type IIn/L) SN template is now excluded due to the fading of the SN. In addition to the SN 1999em template, we have now also compared the NIR light curve of SN 2011hi with that of other Type IIP SNe: 2003hn (Krisicunas et al. 2009) and 2004et (Maguire et al. 2010). The results of the best fits are similar to those obtained with SN 1999em, but having larger  $\chi^2$  values. The V-band extinctions from the three different Type IIP SNe used for comparison are consistent within 0.5 mag for the adopted extinction law. We conclude that SN 2011hi was in fact a slightly over-luminous (1–2 mag brighter than SN 1999em) Type IIP SN discovered roughly a month after the explosion, with 5 or 7 mag of host galaxy extinction in the V-band adopting either the Cardelli et al. (1989) or the Calzetti et al. (2000) reddening law, respectively.

There are no radio sources detected with the e-EVN above  $3\sigma$  at/around the reported positions for either SN 2010cu, nor SN 2011hi. Therefore, the  $3\sigma$  upper limits at 5 GHz correspond to  $2.4 \times 10^{27} \text{ erg s}^{-1} \text{ Hz}^{-1}$  for both SNe. The SNe are also not detected in the archival 8.4 GHz VLBA observations (project BC196) carried out two months after our e-EVN observations. Source B2a detected with e-MERLIN at 6.9 GHz is positionally consistent within the uncertainties with SN 2010cu. However, B2a is not a compact source, and we thus discard the possibility of it being a SN.

SN 2010cu, has an estimated age of 14–17 months at the time of the radio observations made in 2011. Its non-detection at 5, 6.9 and 8.4 GHz is an indication that: (i) the radio emission at these frequencies was well into the optically thin decline phase of its evolution (e.g., a Type Ib/c SN), now having a luminosity well below  $2.4 \times 10^{27} \text{ erg s}^{-1} \text{ Hz}^{-1}$ ; and/or (ii) SN 2010cu is an intrinsically low-luminosity Type II radio supernova (e.g., a Type IIP such as SN 1999em) and thus more sensitive observations would be required for its detection.

SN 2011hi was also not detected in our radio observations made 2–5 months after its explosion, and this is consistent with the fact that type IIP SNe are low-luminosity radio emitters. In fact, other well known type IIP SNe like SN 1999em, 2004dj, and 2004et (Pooley et al. 2002; Beswick et al. 2005; Martí-Vidal et al. 2007, respectively) have peak radio luminosities below  $10^{26} \text{ erg s}^{-1} \text{ Hz}^{-1}$  (see e.g., figure 2 in Chevalier et al. 2006). At NIR wavelengths SN 2011hi was only slightly brighter than SN 1999em; if its radio emission was likewise only slightly stronger, we can expect that its radio luminosity was well below the  $3\sigma$  detection threshold ( $2.4 \times 10^{27} \text{ erg s}^{-1} \text{ Hz}^{-1}$ ) of our most sensitive radio observations carried out with the e-EVN. We note that the non-detection of SNe 2010cu and 2011hi at radio wavelengths does not imply that no radio emission has been produced by these NIR detected SNe.

To gain a better understanding of SNe in LIRGs, it is desirable to have a radio monitoring of the NIR-detected SNe including observations at different frequencies over many epochs. This strategy would help to detect either a fast or a slowly-evolving SN, which can also help to constrain their type (Stockdale et al. 2007). However, not all CCSNe will be bright radio emitters. This depends on the interaction between the SN ejecta and the

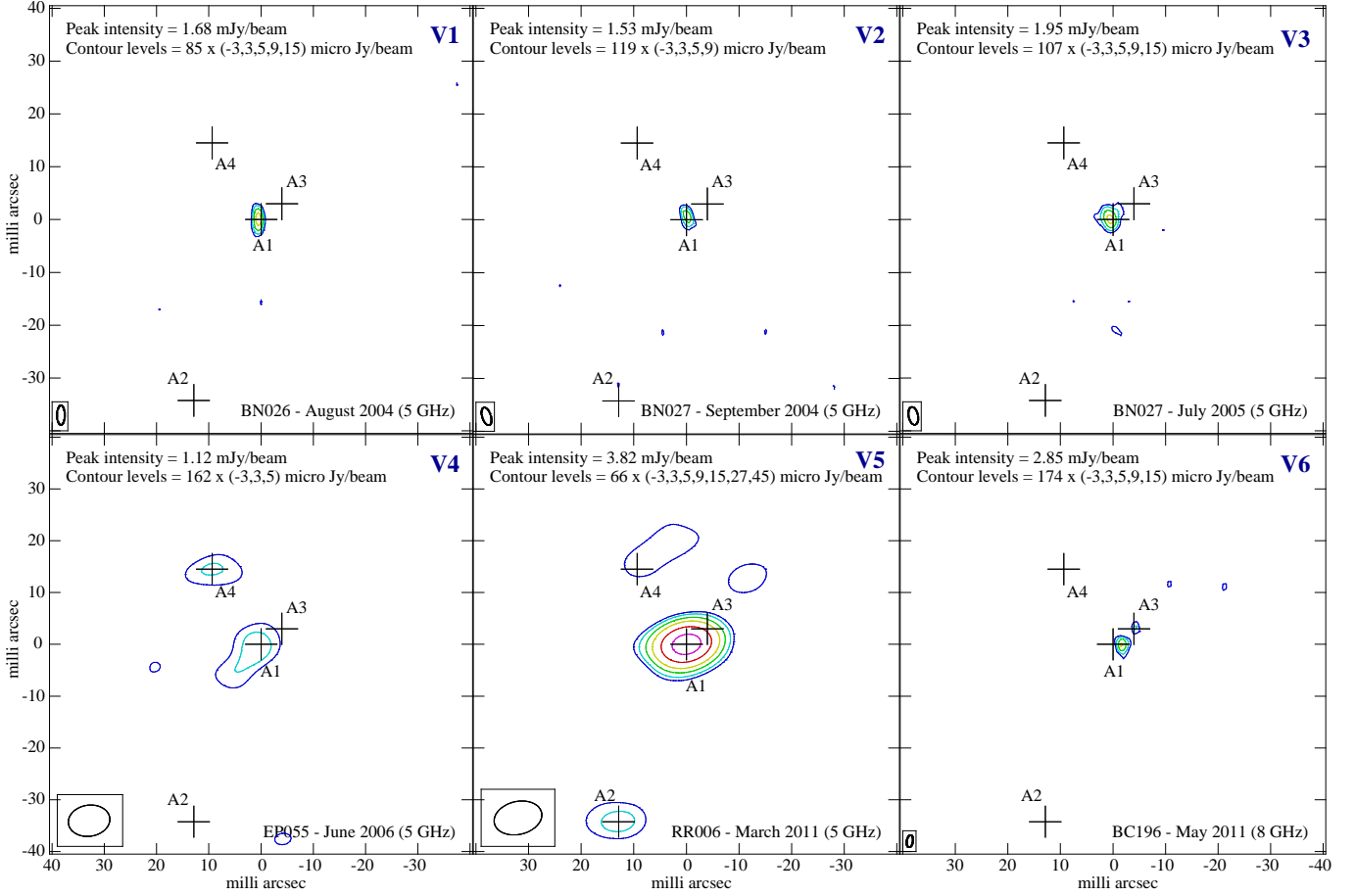


**Fig. 2.** IC 883 contour maps of the VLBI observations listed in Table 1. All the maps are centred on  $\alpha(\text{J2000}) = 13^{\text{h}}20^{\text{m}}35^{\text{s}}.3184$ ,  $\delta(\text{J2000}) = 34^{\circ}08'22''.352$ . The crosses indicate the positions from the detection epoch of the different  $5\sigma$  sources reported in Table 2: A1 and A2 from experiment V5; A3 from experiment V6; and A4 from experiment V4.

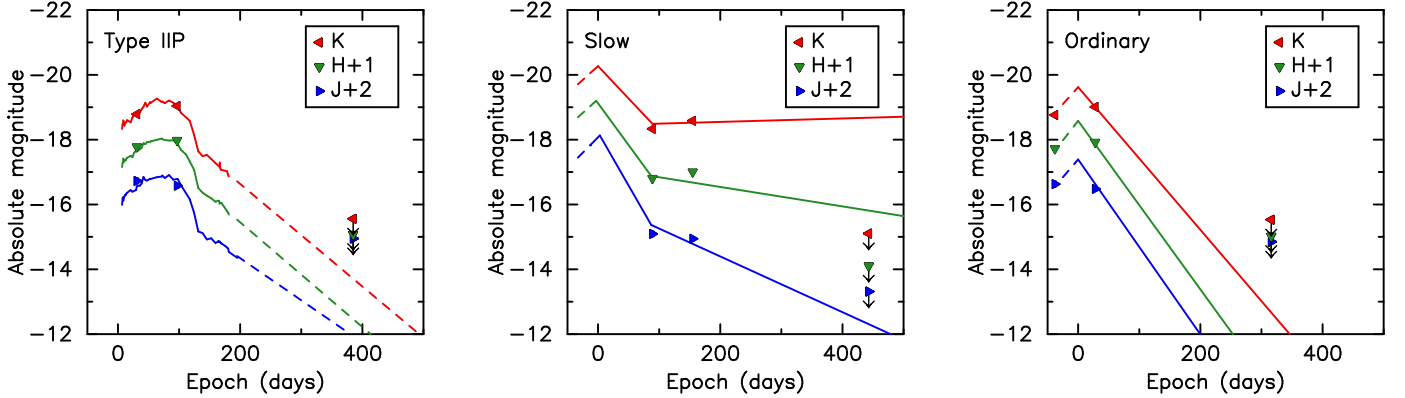


**Fig. 3.** Template light curve fits for SN 2011hi presented in Kankare et al. (2012) adopting the Calzetti et al. (2000) extinction law, with the addition of the late time *JHK* upper limits obtained for SN 2011hi in this work. The epochs not covered by the templates are linearly extrapolated and marked with the dashed lines.

circumstellar medium, which gives rise to the synchrotron emission at radio frequencies (see e.g., Chevalier 1982).

### 3.2. The circumnuclear regions of IC 883: a jet or a disk?

The quest to detect radio emission from SNe 2010cu and 2011hi has brought the opportunity to unveil different facets of IC 883.

In the following we discuss the circumnuclear structure of IC 883 and the nature of its nuclear regions.

Our e-MERLIN observations reveal a double-sided structure with an approximate projected extent of 2 arcsec ( $\sim 1$  kpc) by 0.3 arcsec ( $\approx 150$  pc), at a position angle of  $130^\circ$  (Figure 1). This inclination matches that previously found in other radio studies (e.g., Condon et al. 1991; Parra et al. 2010). However, the double-sided structure in IC 883 is revealed for the first time at 6.9 GHz with our e-MERLIN observations (see also the 1.4 GHz

**Table 2.** Estimated parameters of the detected radio emitting sources in the (circum-)nuclear regions of IC 883.

Source name	Epoch label	$\Delta\alpha''(J2000)$	$\Delta\delta''(J2000)$	$P_\nu$ (mJy/beam)	$S_\nu$ (mJy)	$L_\nu$ ( $10^{27}$ erg s $^{-1}$ Hz $^{-1}$ )	$\Theta_M \times \Theta_m$ (mas $^2$ )	$\log T_B$ (K)
(1)	(2)	(3)	(4)	(5)	(6)	(7)	(8)	(9)
A	EM	35.319 (<1)	22.35 (1)	$4.89 \pm 0.25$	$6.07 \pm 0.31$	$72.65 \pm 3.67$	$104.8 \times 30.4$	$4.15 \pm 0.02$
B1a	EM	35.332 (1)	22.15 (3)	$1.04 \pm 0.07$	$2.07 \pm 0.11$	$24.75 \pm 1.34$	$138.1 \times 97.1$	$3.45 \pm 0.02$
B1b	EM	35.304 (1)	22.63 (6)	$0.59 \pm 0.05$	$1.75 \pm 0.10$	$20.97 \pm 1.17$	$191.3 \times 141.6$	$3.09 \pm 0.02$
B2a	EM	35.356 (1)	21.74 (3)	$1.03 \pm 0.07$	$2.54 \pm 0.13$	$30.34 \pm 1.61$	$224.0 \times 90.5$	$3.11 \pm 0.02$
B2b	EM	35.281 (2)	23.05 (11)	$0.31 \pm 0.05$	$0.97 \pm 0.07$	$11.55 \pm 0.78$	$295.9 \times 109.8$	$2.45 \pm 0.03$
A1	V1	31.3180 (~0.0)	22.352 (0.1)	$1.68 \pm 0.12$	$1.94 \pm 0.13$	$23.19 \pm 1.54$	$1.2 \times 0.6$	$7.81 \pm 0.03$
	V2	31.3179 (0.1)	22.352 (~0.0)	$1.53 \pm 0.14$	$1.53 \pm 0.14$	$18.33 \pm 1.69$	$0.6 \times \dots$	$6.79 \pm 0.04$
	V3	35.3181 (0.1)	22.349 (0.1)	$1.95 \pm 0.15$	$2.65 \pm 0.17$	$31.73 \pm 2.04$	$1.8 \times 0.3$	$7.59 \pm 0.03$
	V4	35.3180 (0.6)	22.351 (~0.0)	$1.12 \pm 0.17$	$1.21 \pm 0.17$	$14.49 \pm 2.07$	$13.0 \times \dots$	$5.97 \pm 0.06$
	V5	35.3179 (0.1)	22.352 (~0.0)	$3.82 \pm 0.20$	$3.82 \pm 0.20$	$45.67 \pm 2.42$	$0.8 \times \dots$	$6.35 \pm 0.02$
	V6	35.3178 (~0.0)	22.351 (0.1)	$2.85 \pm 0.22$	$4.38 \pm 0.28$	$52.34 \pm 3.34$	$1.5 \times 0.4$	$7.55 \pm 0.03$
A2	V5	35.3190 (0.7)	22.317 (0.2)	$0.42 \pm 0.07$	$0.56 \pm 0.07$	$6.66 \pm 0.86$	$7.0 \times 2.0$	$5.75 \pm 0.06$
A3	V6	35.3176 (~0.0)	22.354 (0.2)	$0.97 \pm 0.18$	$1.55 \pm 0.19$	$18.54 \pm 2.28$	$1.4 \times 1.1$	$7.15 \pm 0.05$
A4	V4	35.3181 (0.7)	22.371 (0.1)	$0.89 \pm 0.17$	$1.27 \pm 0.17$	$15.25 \pm 2.08$	$8.1 \times 0.6$	$5.98 \pm 0.06$
	V5	35.3187 (0.9)	22.366 (0.2)	$0.33 \pm 0.07$	$0.67 \pm 0.07$	$8.06 \pm 0.89$	$14.0 \times 1.4$	$5.23 \pm 0.05$

**Notes.** *Columns:* (1) Source names corresponding to those in Figures 1 and 2. (2) Epoch label corresponding to those specified in Table 1. Note that epoch EM and V5 are quasi-simultaneous. (3–4) Coordinates given with respect to  $\alpha(J2000) = 13^h20^m00^s.0$  and  $\delta(J2000) = 34^\circ08'00''.0$ . Position uncertainties in mas, within parentheses, are given by  $\text{FWHM}/(2 \times \text{SNR})$ , where  $\text{SNR}$  is the signal to noise ratio, and FWHM was taken as the projection of the beam major axis on both  $\alpha$  and  $\delta$  axes. (5) Peak intensity. We estimated the uncertainties by adding in quadrature the rms noise in the map (column 10 in Table 1) plus a 5% uncertainty in the point source flux density calibration. (6) Flux density. (7) Monochromatic luminosity at the observed frequency (column 5 in Table 1). (8) Deconvolved major and minor axes, obtained by fitting a Gaussian to each source. (9) Brightness temperature. When no deconvolved sizes could be obtained, we used instead the solid angle subtended by the synthesised beam for calculating lower limits of  $T_B$ , i.e.,  $\Omega_s = \pi(4\log 2)^{-1}(\text{FWHM}_M \times \text{FWHM}_m)$ , with  $\text{FWHM}_M$  and  $\text{FWHM}_m$ , the major and minor synthesised beam fitted FWHM (column 9 in Table 1), respectively.

MERLIN map from Clemens & Alexander 2004). VLA observations (e.g., from Condon et al. 1991; Parra et al. 2010) do not have enough spatial resolution to image the circumnuclear regions with similar level of detail. By convolving our e-MERLIN image with a beam of size  $0''.4$ , which corresponds to VLA A-configuration observations at 5 GHz, we were able to recover a structure similar to that shown in figure 2 from Parra et al. (2010).

At first glance, the structure seen with e-MERLIN resembles that of a two-sided jet of an AGN, whose restarting activity explains the presence of two sets of condensations (B1a-B1b and B2a-B2b; see left panel in Figure 1), at either side of the core A. The larger flux density of the approaching components in the jet, B1a and B2a in this case, with respect to the flux density of the receding components, B1b and B2b, could be explained by Doppler boosting effects.

There are however strong arguments against a jet interpretation: (i) the approaching components are at shorter distances from the core than the receding components, thus implying that their apparent velocities are smaller; (ii) the putative jet structure is placed on top of the disk of the galaxy, and this is difficult to explain, unless we consider that the directions of jet and disk coincide due to a projection effect.

Different studies of the molecular and atomic gas towards IC 883 (Downes & Solomon 1998; Bryant & Scoville 1999; Clemens & Alexander 2004), give evidence of the rotation of the disk from South-East towards North-West. This situation would imply that the putative jet is perpendicular to the rotation axis, and hence no projection effect could explain the superposition of the jet on the disk. Schmitt et al. (2002) studied the orientation of jets with respect to the rotation axis in a sample of radio galaxies and found that large misalignments ( $< 77^\circ$ ) may occur due to warping mechanisms in the black hole's accretion disk. In the case of IC 883 the misalignment would be close to  $90^\circ$ , so

a jet scenario for the structure revealed with e-MERLIN is even less viable.

If we consider instead a rotating disk (or ring) scenario, component A would be at the centre, while B1a, B2a (approaching components) and B1b, B2b (receding components) would be continuum radio components of the disk itself. We note that the line joining component B1a with B1b through A, is not the same as the line joining B2a with B2b, which gives evidence of the disk/ring being warped (in agreement with previous studies, e.g., Clemens & Alexander 2004), probably due to the interaction with the ambient material. We note that the structure unveiled by e-MERLIN has a width of approximately 150 pc. Whilst such width might appear too narrow for representing a disk, thin disks of a few hundreds of parsecs are not uncommon for edge-on galaxies at radio frequencies (Dumke et al. 1995). Furthermore, e-MERLIN resolves out some of the extended emission which is otherwise visible at lower resolution, for instance with the VLA (Condon et al. 1991; Parra et al. 2010), and hence, the size of the structure mapped with e-MERLIN is compatible with a disk/ring structure.

Thus, whilst we cannot completely rule out the possibility that the structure mapped by e-MERLIN is a jet, there is strong evidence against it, and evidence favouring a rotating disk/ring nature instead.

Further e-MERLIN observations at different frequencies could be used to probe the radio lifetime of the condensations at either side of the core A. Observations optimized for polarimetry studies would yield information on the configuration of the large-scale magnetic field, which could probe the existence of shocked material as expected in a jet scenario, hence helping to arrive to a firm conclusion.

### 3.3. The ongoing nuclear activity in IC 883

Our e-EVN observations (see right panel in Figure 1), made simultaneous to our e-MERLIN observations, reveal the presence of at least two compact sources (labelled as A1 and A2) above  $5\sigma$  in the innermost nuclear regions of IC 883. The high brightness temperature of sources A1 and A2 indicates a non-thermal origin for both of them.

The brightest component in our e-MERLIN image (A) has a peak intensity similar to that of A1. By adding up the flux densities of components A1 and A2 in our e-EVN map, we recover a flux density of  $4.38 \pm 0.27$  mJy, which is still lower than both the peak intensity and the flux density of component A (see Table 2). We find that A1 has a strong contribution to the flux density at larger scales (although seen at slightly different frequencies), and furthermore, has a position highly coincident with component A, despite the use of different phase reference sources and different spatial resolutions. Hence, A1 is very likely the main powering source for the radio emission of component A.

From our e-EVN observations alone we cannot characterise the nature of sources A1 and A2, nor investigate a possible relation between components A1 and A. We have therefore searched for additional, publicly available, archival VLBI data (see Table 1) that could be of use to investigate these issues.

Component A1 from our e-EVN observations is detected in all the additional VLBI observations (see Figure 2) and appears to fluctuate in flux density at 5 GHz, varying for at least a factor of three between the minimum and maximum value displayed within the seven years comprised by the different VLBI epochs (see Table 2). Component A2 is not detected in any other epoch. At 8.4 GHz (experiment BC196) we detect a  $5\sigma$  source (A3) North-West of component A1. The resolution of our e-EVN observations (RR006) does not allow us to detect component A3, but the source is also not detected in any of the other VLBA epochs at 5 GHz, which have a resolution similar to that of experiment BC196. A  $3\sigma$  component placed North-East from component A1, is detected as a  $5\sigma$  source in experiment EP055 and is labelled as A4. This source has no counterpart at 8.4 GHz in the observations under project BC196, indicating that at that frequency the emission from A4 has become optically thin, as expected in a SN scenario. We thus have a total of three transient sources (A2, A3 and A4) in the nucleus of IC 883, in addition to the more luminous, variable, component A1, which has remained visible for at least seven years.

### 3.4. The nature of the compact sources in the IC 883 nucleus

The milliarcsec sources detected in the innermost regions of IC 883 give evidence of its ongoing nuclear activity. A variable source, A1, has been detected in six different VLBI epochs (see Table 2 and Figure 2) throughout seven years, and appears to be the main powering source of the emission at larger scales imaged with e-MERLIN. Three transient sources have also been detected. All the sources have sizes and brightness temperatures indicating a non-thermal origin. The transient sources are most probably SNe and/or SN remnants (SNR), whereas for component A1 the nature is less clear. To investigate the nature of sources A1–A4, we compare their luminosities with those reported in the literature for the non-thermal sources (SNe and SNRs) at 5 GHz in the starburst galaxy M82, the LIRG Arp 299-A and in the ULIRG Arp 220 (Figure 4).

From Figure 4 we see that the nuclear components of IC 883, although being less numerous, are in general more luminous than the components identified as SNe and SNRs in the nuclear re-

gions of other galaxies with high star formation rates. The lifetime of the transient sources in IC 883 ranges from less than a few months up to a few years. It is thus very likely that these sources are a mixture of SNe and SNRs, therefore indicating a recent starburst activity in the nucleus of IC 883. We lack spectral information that could have helped to differentiate between a SN or a SNR origin for each of these transient sources.

Component A1 is the most luminous of all the sources (see histogram in Figure 4). A SN or a SNR origin are not very likely, based on its flux density fluctuations (see columns 5 and 6 in Table 2), its longevity, and its relatively flat two-point spectral index between 5 and 8.4 GHz,  $\alpha = 0.3$  ( $S_\nu \sim \nu^\alpha$ ), calculated from the flux densities obtained in experiments RR006 and BC196. Therefore A1 is very likely an AGN.

Further evidence for an obscured AGN in IC 883 can be inferred from the ratio of radio to hard X-ray luminosity ( $R_X = \nu L_\nu(5 \text{ GHz})/L_{\text{HX}}$ ; Terashima & Wilson 2003). Iwasawa et al. (2011) report a hard X-ray luminosity ( $L_{\text{HX}} = L[2\text{--}10 \text{ keV}]$ ) of  $6.4 \times 10^{40} \text{ erg s}^{-1}$  for IC 883. Considering the luminosity at 5 GHz of A1 observed with the e-EVN (see Table 2), we calculate  $R_X \approx 3.6 \times 10^{-3}$ , which is consistent with a low-luminosity AGN (LLAGN) or a normal AGN in a radio galaxy, as inferred from figure 4 of Terashima & Wilson (2003).

By comparing the maximum variability (a factor of  $\sim 3$ ) displayed by A1 in our observations, with the largest inter-year variability displayed by typical LLAGNs (Nagar et al. 2002), we find that A1 would be placed at the high end of the LLAGN behaviour. Thus, we can only conclude that A1 is a candidate for either a normal AGN or a low-luminosity one.

Component A4 whose elongation could indicate a sort of outflow, has however no counterpart at 8.4 GHz (experiment BC196). Future VLBI observations at different frequencies should allow an unequivocal characterisation of the AGN candidate in IC 883, as well as possibly discovering further nuclear components.

If we consider sources A2, A3 and A4 as having their origin in recent star formation activity, we would have three CCSN events that have occurred in the period between June 2006 and May 2011, i.e., five years. We can thus estimate a CCSN rate for the IC 883 nuclear region of  $\approx 0.6_{-0.3}^{+0.6} \text{ yr}^{-1}$ , using the upper and lower Poisson  $1\sigma$  uncertainties for three events given by Gehrels (1986). Combining the nuclear CCSN rate with the CCSN rate inferred from the detection of SNe 2010cu and 2011hi within 3.8 yr in the circumnuclear regions of IC 883, we obtain a CCSN rate for the entire galaxy of  $\approx 1.1_{-0.6}^{+1.3} \text{ yr}^{-1}$ . These rates are considered as lower limits since our irregular temporal sampling both at radio and at NIR wavelengths might have missed rapidly evolving SNe, and also because our  $5\sigma$  radio luminosity detection threshold ( $4 \times 10^{27} \text{ erg s}^{-1} \text{ Hz}^{-1}$ ) prevents us from detecting Type IIP and IIB SNe, and even some Type IIL. We note that the total rate estimate is in agreement with the IR luminosity-based CCSN rate estimate (see Section 1). It is thus of great interest to estimate the contribution of a putative AGN to the IR luminosity in order to obtain a more reliable estimate of the expected CCSN rate.

### 3.5. The infrared SED of IC 883: estimating the contribution of an AGN

As mentioned in Section 1, IC 883 has been classified as a composite starburst-AGN, based on optical diagnostic diagrams (Yuan et al. 2010).

We have modelled the spectral energy distribution (SED) of IC 883 (see Figure 5) to estimate the contribution of an

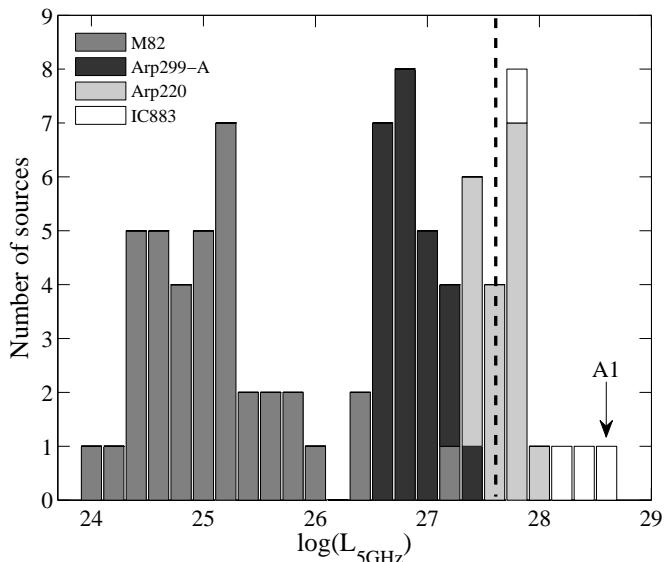


**Fig. 4.** Luminosity distribution at 5 GHz of SNe and SNRs in M82, Arp 299-A, Arp 220. All the IC 883 nuclear sources have been added for comparison purposes. Each bin has a width of  $\log_{10}(L_{5\text{GHz}}) = 0.2$  with  $L_{5\text{GHz}}$  in units of  $\text{erg s}^{-1} \text{Hz}^{-1}$ . The SN and SNR luminosities have been retrieved from Fenech et al. (2008) and Marchili et al. (2010) for M82, Bondi et al. (2012) for Arp 299-A and from Batejat et al. (2011) for Arp 220. The most luminous M82 source corresponds to SN 2008iz. In the case of Arp 220 we have included SNe and SNRs from both West and East nuclei. The luminosities of the IC 883 components were taken from Table 2: from experiment RR006 for A1 and A2, from experiment BC196 for A3, and from experiment EP055 for A4. We have assumed a spectral index of  $-0.7$  to obtain the luminosity at 5 GHz of component A3. Note that A1 is the brightest source, and with our most sensitive VLBI image (RR006) we are only sensitive to sources above a  $5\sigma$  luminosity limit of  $4 \times 10^{27} \text{erg s}^{-1} \text{Hz}^{-1}$ , indicated by a dashed line in the histogram.

AGN to the total IR luminosity and to provide an estimate for the CCSN rate in this galaxy. For this we used a grid of AGN dusty torus models that have been computed with the method of Efstathiou & Rowan-Robinson (1995) and a grid of starburst models that have been computed with the method of Efstathiou et al. (2000), but with a revised dust model (Efstathiou & Siebenmorgen 2009). The spatial resolution of the mid- and far-IR data used for the modelling is not high enough to spatially separate the different components. Therefore to distinguish the contribution of the AGN torus and the starburst we have fitted a model combining both an AGN and a starburst.

For the AGN, we considered a grid of tapered disc models computed with the method of Efstathiou & Rowan-Robinson (1995). In this grid of models we consider four discrete values for the equatorial  $1000 \text{ \AA}$  optical depth (500, 750, 1000, 1250), three values for the ratio of outer to inner disc radii (20, 60, 100) and three values for the opening angle of the disc ( $30^\circ$ ,  $45^\circ$  and  $60^\circ$ ). The best fit parameters which resulted in the minimum  $\chi^2$  when we combine the starburst and the AGN torus models, are an opening angle of  $60^\circ$  for the torus, an equatorial optical depth of 1250 at  $1000 \text{ \AA}$ , and a ratio of outer to inner radius of 60. The AGN torus is viewed close to edge-on due to the IC 883 geometry; thus, its apparent contribution to the total infrared emission

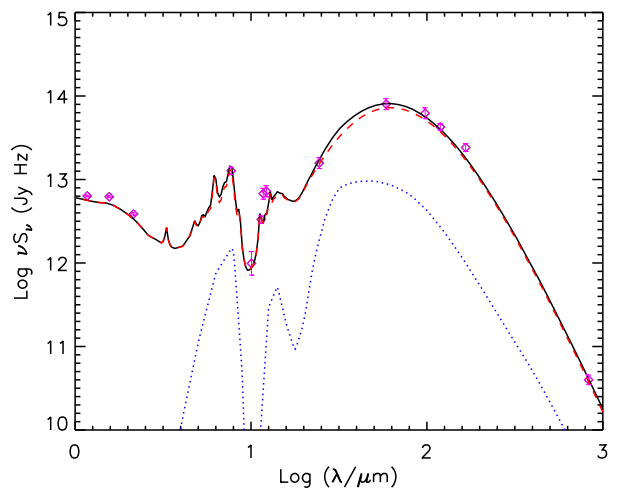


**Fig. 5.** The infrared SED of IC 883 including 2MASS and IRAS data, as well as the SCUBA point from Dunne et al. (2000). The red-dashed line is our starburst model fit, and the blue-dotted line is the model fit for an AGN upper limit contribution. The black-solid line is the model fit including both components.

is insignificant (probably  $<10$  per cent of the starburst luminosity). Therefore the starburst clearly dominates the observed luminosity of the entire galaxy. We note that due to viewing the torus almost edge-on and due to its extremely high optical depth, the intrinsic luminosity of the AGN itself could be a factor of  $\sim 30$  times higher than the observed one. This enhancing factor is related to the anisotropy of the torus emission (see Efstathiou 2006, for a definition), and implies that the intrinsic luminosity of the AGN could be about three times higher than the observed starburst luminosity.

Our model incorporates the stellar population synthesis model of Bruzual & Charlot (2003), which makes a prediction of the SN rate,  $\nu_{\text{SN}}(t)$ , at a time  $t$  after star formation in an instantaneous burst. The starburst model of Efstathiou et al. (2000) predicts the spectrum of this instantaneous burst at time  $t$  and assumes a star formation history for the starburst. We assume that the SFR in IC 883 declines exponentially with an e-folding time of 20 Myr, and that the age of the starburst is 55 Myr. The initial optical depth of the molecular clouds that constitute the starburst is assumed to be 100. The SFR averaged over the duration of the starburst is  $185 M_{\odot} \text{yr}^{-1}$ . It is also possible to calculate self-consistently SN rate at different stages in the evolution of a starburst by convolving the star formation history with  $\nu_{\text{SN}}(t)$ . This yields a  $\nu_{\text{SN}}$  of  $1.1 \text{ yr}^{-1}$  which is relevant for the entire galaxy and can therefore be compared with the observed values. The combination of the CCSN rate for the circumnuclear regions based on three radio SNe, and the CCSN rate for the circumnuclear regions based on the discovery of SNe 2010cu and 2011hi, resulted in a lower limit for the CCSN rate of  $\approx 1.1^{+1.3}_{-0.6} \text{ yr}^{-1}$  for the entire galaxy (see Section 3.4). This CCSN rate estimate is in good agreement with the predicted CCSN rate for the entire IC 883 galaxy from the IR SED modelling.

IC 883 being less luminous in the IR, but farther away than Arp 299-A and in a much more advanced merger stage, contains both a starburst and an AGN. The nuclear starburst in IC 883 is apparently less prolific than in Arp 299-A (Pérez-Torres et al. 2009). However, the AGN in IC 883 seems to be stronger than the one in Arp 299-A (Pérez-Torres et al. 2010), and even powering the radio luminosity at circumnuclear scales, although its



contribution to the emission of the entire galaxy at IR wavelengths is apparently insignificant.

#### 4. Summary

We have imaged the nuclear and circumnuclear regions of the LIRG IC 883 at radio frequencies. Our e-EVN observations, together with archival VLBI observations, reveal the presence of at least four non-thermal components in the nuclear regions of IC 883. Three of these are transient sources and one is a long-lived, variable compact source, which is very likely an AGN. Our e-MERLIN observations highlight the presence of a striking double-sided structure, likely representing a warped disk/ring, in agreement with previous studies on the interstellar medium of this galaxy.

The source we identify as an AGN candidate is powering the radio emission in IC 883 at nuclear and circumnuclear scales, and yet, as indicated by our radio and NIR observations, as well as by our model of the IR SED, this LIRG displays very active star formation both within the innermost 100 pc of its nucleus, and in the circumnuclear regions. We have estimated lower limits for the CCSN rate in the innermost nuclear regions of  $0.6^{+0.6}_{-0.3} \text{ yr}^{-1}$  based on the detection of three radio SNe above a  $5\sigma$  luminosity threshold of  $4 \times 10^{27} \text{ erg s}^{-1} \text{ Hz}^{-1}$ , and  $1.1^{+1.3}_{-0.6} \text{ yr}^{-1}$  for the entire galaxy, based on the nuclear radio SNe and the NIR SNe 2010cu and 2011hi discovered in the circumnuclear regions. Our most recent NIR Gemini-North observations of IC 883 clarify the nature of SN 2011hi as a Type IIP SN, in agreement with its non-detection in our observations at radio frequencies.

The composite starburst-AGN nature of IC 883, revealed previously by optical spectroscopy (e.g., Yuan et al. 2010), is now supported by our radio observations for the first time, thus making IC 883 one of the few galaxies where the starburst-AGN connection can be studied in detail.

*Acknowledgements.* We thank the anonymous referee for his/her comments. The authors are thankful to the EVN Directors for their rapid response for ToO observations. The European VLBI Network is a joint facility of European, Chinese, South African and other radio astronomy institutes funded by their national research councils. We also made use of observations with e-MERLIN, the UK's facility for high resolution radio astronomy observations, operated by The University of Manchester for the Science and Technology Facilities Council; and observations obtained at the Gemini Observatory, which is operated by the Association of Universities for Research in Astronomy, Inc., under a cooperative agreement with the NSF on behalf of the Gemini partnership: the National Science Foundation (United States), the Science and Technology Facilities Council (United Kingdom), the National Research Council (Canada), CONICYT (Chile), the Australian Research Council (Australia), Ministério da Ciência e Tecnologia (Brazil) and Ministerio de Ciencia, Tecnología e Innovación Productiva (Argentina). This article is also based on observations made with the Very Long Baseline Array (VLBA) of the National Radio Astronomy Observatory (NRAO); the NRAO is a facility of the National Science Foundation operated under cooperative agreement by Associated Universities, Inc. This work made use of the Swinburne University of Technology software correlator, developed as part of the Australian Major National Research Facilities Programme and operated under licence. Our work is supported by the European Community Framework Programme 7, Advanced Radio Astronomy in Europe, grant agreement no.: 227290. C.R.-C., M.A.P.-T. and A.A. acknowledge financial support from the Spanish MICINN through grant AYA2009-13036-C02-01, co-funded with FEDER funds. S.M., E.K. and C.R.-C. acknowledge financial support from the Academy of Finland (project: 8120503). E.K. acknowledges support from the Finnish Academy of Science and Letters (Vilho, Yrjö and Kalle Väisälä Foundation).

#### References

Alard, C. 2000, *A&AS*, 144, 363  
Alard, C. & Lupton, R. H. 1998, *ApJ*, 503, 325

Batejat, F., Conway, J. E., Hurley, R., et al. 2011, *ApJ*, 740, 95  
Beswick, R. J., Muxlow, T. W. B., Argo, M. K., et al. 2005, *ApJ*, 623, L21  
Bondi, M., Pérez-Torres, M. A., Herrero-Illana, R., & Alberdi, A. 2012, *A&A*, 539, A134  
Bruzual, G. & Charlot, S. 2003, *MNRAS*, 344, 1000  
Bryant, P. M. & Scoville, N. Z. 1999, *AJ*, 117, 2632  
Calzetti, D., Armus, L., Bohlin, R. C., et al. 2000, *ApJ*, 533, 682  
Cardelli, J. A., Clayton, G. C., & Mathis, J. S. 1989, *ApJ*, 345, 245  
Chevalier, R. A. 1982, *ApJ*, 259, 302  
Chevalier, R. A., Fransson, C., & Nymark, T. K. 2006, *ApJ*, 641, 1029  
Clemens, M. S. & Alexander, P. 2004, *MNRAS*, 350, 66  
Condon, J. J., Huang, Z.-P., Yin, Q. F., & Thuan, T. X. 1991, *ApJ*, 378, 65  
Deller, A. T., Brisken, W. F., Phillips, C. J., et al. 2011, *PASP*, 123, 275  
Downes, D. & Solomon, P. M. 1998, *ApJ*, 507, 615  
Dumke, M., Krause, M., Wielebinski, R., & Klein, U. 1995, *A&A*, 302, 691  
Dunne, L., Eales, S., Edmunds, M., et al. 2000, *MNRAS*, 315, 115  
Efstathiou, A. 2006, *MNRAS*, 371, L70  
Efstathiou, A. & Rowan-Robinson, M. 1995, *MNRAS*, 273, 649  
Efstathiou, A., Rowan-Robinson, M., & Siebenmorgen, R. 2000, *MNRAS*, 313, 734  
Efstathiou, A. & Siebenmorgen, R. 2009, *A&A*, 502, 541  
Fenech, D. M., Muxlow, T. W. B., Beswick, R. J., Pedlar, A., & Argo, M. K. 2008, *MNRAS*, 391, 1384  
Gehrels, N. 1986, *ApJ*, 303, 336  
Iwasawa, K., Sanders, D. B., Teng, S. H., et al. 2011, *A&A*, 529, A106+  
Kankare, E., Mattila, S., Ryder, S., et al. 2008, *ApJ*, 689, L97  
Kankare, E., Mattila, S., Ryder, S., et al. 2012, *ApJ*, 744, L19  
Kankare, E., Ryder, S. D., Mattila, S., et al. 2011, Central Bureau Electronic Telegrams, 2889, 1  
Keel, W. C. 1985, *AJ*, 90, 2207  
Kewley, L. J., Groves, B., Kauffmann, G., & Heckman, T. 2006, *MNRAS*, 372, 961  
Krisциunas, K., Hamuy, M., Suntzeff, N. B., et al. 2009, *AJ*, 137, 34  
Maguire, K., Di Carlo, E., Smartt, S. J., et al. 2010, *MNRAS*, 404, 981  
Marchili, N., Martí-Vidal, I., Brunthaler, A., et al. 2010, *A&A*, 509, A47+  
Martí-Vidal, I., Marcaide, J. M., Alberdi, A., et al. 2007, *A&A*, 470, 1071  
Mattila, S. & Meikle, W. P. S. 2001, *MNRAS*, 324, 325  
Modica, F., Vavilkin, T., Evans, A. S., et al. 2012, *AJ*, 143, 16  
Nagar, N. M., Falcke, H., Wilson, A. S., & Ulvestad, J. S. 2002, *A&A*, 392, 53  
Parra, R., Conway, J. E., Aalto, S., et al. 2010, *ApJ*, 720, 555  
Pérez-Torres, M. A., Alberdi, A., Romero-Cañizales, C., & Bondi, M. 2010, *A&A*, 519, L5+  
Pérez-Torres, M. A., Romero-Cañizales, C., Alberdi, A., & Polatidis, A. 2009, *A&A*, 507, L17  
Pooley, D., Lewin, W. H. G., Fox, D. W., et al. 2002, *ApJ*, 572, 932  
Ryder, S., Kankare, E., & Mattila, S. 2010, Central Bureau Electronic Telegrams, 2286, 1  
Sanders, D. B., Mazzarella, J. M., Kim, D., Surace, J. A., & Soifer, B. T. 2003, *AJ*, 126, 1607  
Sanders, D. B. & Mirabel, I. F. 1996, *Annual Review of Astron and Astrophys*, 34, 749  
Schmitt, H. R., Pringle, J. E., Clarke, C. J., & Kinney, A. L. 2002, *ApJ*, 575, 150  
Scoville, N. Z., Evans, A. S., Thompson, R., et al. 2000, *AJ*, 119, 991  
Shepherd, M. C., Pearson, T. J., & Taylor, G. B. 1995, in *Bulletin of the American Astronomical Society*, Vol. 27, *Bulletin of the American Astronomical Society*, ed. B. J. Butler & D. O. Muhleman, 903+  
Smith, D. A., Herter, T., Haynes, M. P., Beichman, C. A., & Gautier, III, T. N. 1995, *ApJ*, 439, 623  
Smith, H. E., Lonsdale, C. J., & Lonsdale, C. J. 1998, *ApJ*, 492, 137  
Stockdale, C. J., Kelley, M. T., Weiler, K. W., et al. 2007, in *American Institute of Physics Conference Series*, Vol. 937, *Supernova 1987A: 20 Years After: Supernovae and Gamma-Ray Bursters*, ed. S. Immler, K. Weiler, & R. McCray, 264–268  
Terashima, Y. & Wilson, A. S. 2003, *ApJ*, 583, 145  
Valenti, S., Fraser, M., Benetti, S., et al. 2011, *MNRAS*, 416, 3138  
Veilleux, S., Kim, D.-C., Sanders, D. B., Mazzarella, J. M., & Soifer, B. T. 1995, *ApJS*, 98, 171  
Yuan, T.-T., Kewley, L. J., & Sanders, D. B. 2010, *ApJ*, 709, 884